Scientific paper

Time-Dependent Structural Analysis Considering Mass Transfer to Evaluate Deterioration Process of RC Structures

Hikaru Nakamura[1], Worapong Srisoros[2], Ryosuke Yashiro[3] and Minoru Kunieda[4]

Received 24 August 2005, accepted 1 November 2005

Abstract

A time-dependent structural analysis method under multi actions in consideration of drying shrinkage due to moisture transfer and rebar corrosion due to chloride ions penetration as well as external load actions was developed. The Rigid-Body-Spring Networks (RBSN) model and the truss networks model were used for structural analysis and mass transfer analysis, respectively. In addition, mass transfer through bulk concrete and mass transfer through cracks by setting truss networks on the boundaries of Voronoi particles, was also considered. The developed method was confirmed to simulate well the deterioration process due to mass transfer for initial cracking behavior and ultimate behavior of concrete structures.

1. Introduction

Cracks in concrete often occur due to the internal stress induced by mass transfer such as moisture and heat or by corrosion expansion of rebar under no external load. Once cracks occur, mass transfer accelerates through the cracks, causing gradual degradation in structural performance and durability. It is, therefore, important to clarify the effect of mass transfer on structural performance and durability in order to assess the service life of concrete structures.

Although the effects of internal stress due to mass transfer have been estimated analytically, the main purpose was to simulate the occurrence of cracks through time. Further, the cracking behavior and other structural performance characteristics such as ultimate behavior have hardly been estimated. On the other hand, although numerical methods for predicting the structural performance of concrete structures before and after the peak load have been advanced, most methods did not consider the continuous effects of initial damage due to mass transfer.

This paper proposes a unified analytical method with load applying analysis for short term behavior and mass transfer analysis for long term behavior under multi actions in consideration of drying shrinkage due to moisture transfer and rebar corrosion due to chloride ion penetration. The Rigid-Body-Spring Networks (RBSN), developed by Kawai (Kawai 1978) is used for structural analysis and the truss networks model is applied for mass transfer analysis. Several analyses in two-dimensions were performed to confirm the effectiveness of the developed method and to simulate the deterioration process induced by mass transfer.

[1]Professor, Department of Civil Engineering, Nagoya University, Nagoya, Japan.
E-mail: hikaru@civil.nagoya-u.ac.jp
[2]Doctoral student, Graduate School, Department of Civil Engineering, Nagoya University, Nagoya, Japan.
[3]Master of Engineering, Graduate School, Department of Civil Engineering, Nagoya University, Nagoya, Japan.
[4]Associate Professor, Department of Civil Engineering, Nagoya University, Nagoya, Japan.

2. Structural analysis

Nowadays, numerical methods for predicting the structural performance of concrete structures are becoming more effective owing to advances in computing technology. The Finite Element Method (FEM) has generally been applied for estimating mechanical behavior of concrete structures. This method provides reasonable prediction for the totality of concrete structure behavior, such as the formation of cracks and load bearing capacity. The deterioration process of concrete structures greatly depends on cracking. Therefore, a model that can accurately simulate crack formation and propagation is required for predicting both the structural performance and durability of concrete structures. Discrete method is better than the continuum models for modeling of material discontinuity. From this viewpoint, the Rigid-Body-Spring Networks approach, which is one of the discrete approaches, is used for structural analysis, since this method is an analytical technique based on discrete mechanics that easily deals with crack propagation of concrete directly (Saito *et al*. 1999).

2.1. Rigid-body-spring networks

Rigid-Body-Spring Networks represent a continuum material as an assembly of rigid particle elements interconnected by zero-size springs along their boundaries. The response of the spring model provides comprehension of the interaction between particles instead of the internal behavior of each particle based on continuum

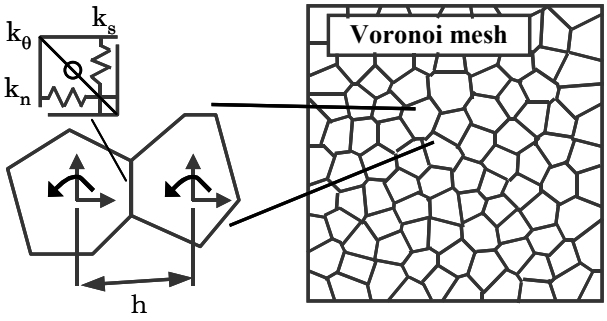

Fig. 1 Rigid-Body-Spring Networks.

mechanics. Each rigid particle has two translations and one rotational degree of freedom defined at the nuclei within. The interface between two particles consists of three individual springs in the normal, tangential and rotations, as shown in **Fig. 1**. Since concrete cracks initiate and propagate along interparticle boundaries, the crack pattern is strongly affected by the mesh design. Therefore, random geometry using Voronoi diagrams (Bolander *et al.* 1998) is applied to partition the material onto an assembly of rigid particle. The random geometry of the networks does not represent any structural feature within the concrete material, but rather is used to reduce mesh bias on potential crack directions.

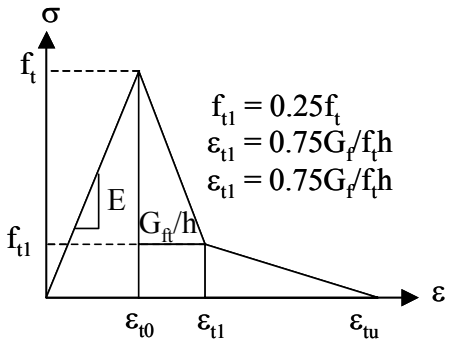

a) Tension (1/4 model)

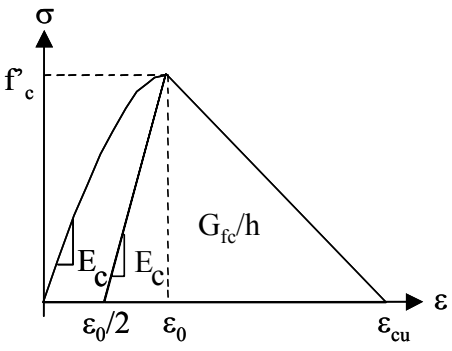

b) Compression (parabolic)

Fig. 2 Stress-strain relationship of concrete.

2.2. Concrete material models

The fracture criterion in RBSN is not based on a tensorial measure of stress, but it uses the average stresses acting normally and tangentially to the particle interface. Normal springs are set to represent the tensile and compressive behavior of concrete.

In this study, the tensile behavior of concrete up to the tensile strength is modeled by using a linear elastic, while a bilinear softening branch of 1/4 model is assumed after cracking, as shown in **Fig. 2 (a)** which is represented by the tensile strength, f_t, the tensile fracture energy, G_{ft}, and the distance between nuclei, h. In this paper, G_{ft} is set to 0.1 N/mm. The behavior of concrete under compressive strength f'_c is modeled using a parabolic curve up to the compressive strength and a linear softening branch is assumed thereafter, as shown in **Fig. 2 (b)**. The slope of the linear softening branch is defined by considering the compressive fracture energy, G_{fc}, of Equation (1) (Nakamura *et al*. 2001) to avoid mesh size dependence as well as tension behavior.

$$G_{fc} = 8.8\sqrt{f'_c} \tag{1}$$

Tangential springs represent the shear transfer mechanism of uncracked and cracked concrete. The shear strength is assumed to the Mohr-Coulomb type criterion with tension and compression caps, as shown in **Fig. 3 (a)**. The cohesion, c, and internal friction angle, ϕ, are set to $0.138f'_c$ and 37°, respectively (Ueda *et al*. 1984). It is assumed that the shear strength is constant when normal stress is greater than $\psi f'_c$, with ψ set to 0.5. After shear stress reaches the yield strength, the stress moves on the

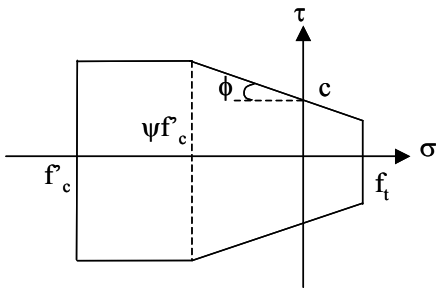

a) Mohr-Coulomb type criteria

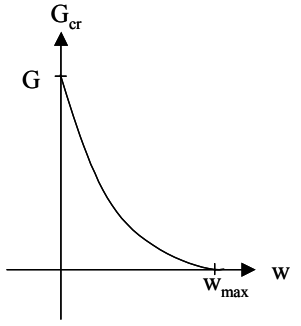

b) Reduction of shear stiffness

Fig. 3 Shear model in concrete.

yield surface until the shear strain reaches the ultimate strain, γ_u. The force in the shear spring is released and the local stiffness, k_t, is set to zero when the shear strain exceeds the ultimate strain. The ultimate strain is set to 0.004 μ in this study. The shear transfer capacity at crack interfaces depends on crack opening. Thus, the shear stress, τ, is calculated by Equation (2) (Saito *et al*. 1999) with the function of the strain of normal spring, ε, Young's modulus, E, and shear strain, γ.

$$\tau = (1-\lambda)\beta G\gamma \tag{2}$$

where

$$\lambda = \begin{cases} 0 & for \quad \gamma \le \gamma_0 \\ 1-\dfrac{\gamma_0}{\gamma}\exp\left[-\dfrac{k}{\gamma_u}(\gamma-\gamma_0)\right] & for \quad \gamma > \gamma_0 \end{cases}$$

$$\beta = \begin{cases} 1 & for \quad \varepsilon \le \varepsilon_{t0} \\ \dfrac{\varepsilon_{t0}}{\varepsilon}\exp\left[-\dfrac{0.3}{\varepsilon_{tu}}(\varepsilon-\varepsilon_{t0})\right] & for \quad \varepsilon > \varepsilon_{t0} \end{cases}$$

where G = shear stiffness and $\gamma_0 = \tau_f/G$. The λ and β parameters represent the degree of damage and reduction factor, respectively, as shown in **Fig. 3 (b)**.

2.3. Reinforcement model

Each reinforcement element is represented by a series of regular beam elements. The beam nodes are attached to the concrete particles without regard to the concrete mesh design through a zero-size link element, as shown in **Fig. 4** (Saito *et al*. 1997). The stress-strain relation of reinforcement is used as a bilinear model. The bond interaction between the concrete and reinforcement strongly affects crack development. The bond stress-slip relation is introduced into the spring parallel to the rebar of the linked elements. **Figure 5** shows the relationship modeled by Equation (3) (Shima *et al*. 1989) up to the bond strength and the same curve as that proposed by

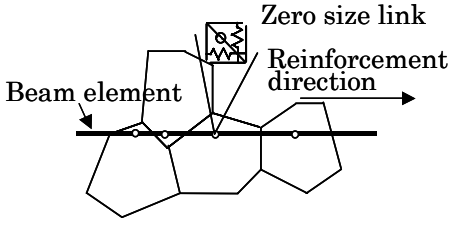

Fig. 4 Reinforcement arrangement.

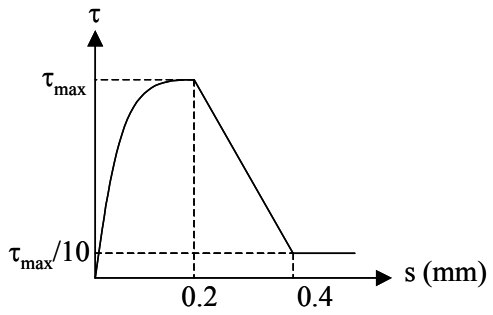

Fig. 5 Bond stress-slip relationship.

CEB-FIB is assumed thereafter (CEB-FIB 1990). Shima *et al*., however, proposed Equation (3) for deformed bars embedded in massive concrete. For application to reinforced concrete beams, which have smaller cover concrete compared to the cover of massive concrete, the reduction factor due to the effect of the concrete covering should also be considered (Kitoku *et al*. 2005). In this paper, this reduction factor, α was set to 0.6.

$$\tau = \alpha 0.9 f_c'^{2/3}\left\{1-\exp\left(-40(s/D)^{0.5}\right)\right\} \tag{3}$$

where s = slip and D = diameter of reinforcement.

Concrete corrosion decreases the effective area of the reinforcement. Furthermore, the bond property between the reinforcement bars and the surrounding concrete is influenced by the corrosion of rebars. However, the reductions in effective area and the change of bond property have not been considered in this paper.

3. Mass transfer analysis

3.1. Truss networks model

Mass transfer is a continuous flow and it is usually analyzed using the same continuum model as that use for the Finite Element approach, which is represented by a partial differential equation, whereas RBSN is used for structural analysis, which does not require continuity. In this section, the truss networks model is used for mass transfer analysis to obtain the initial strain for structural analysis by using RBSN with Voronoi diagrams. Each of the Voronoi elements is linked by truss elements with the

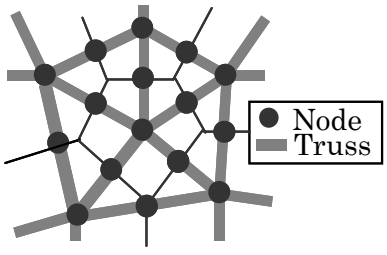

Fig. 6 Truss networks model.

nodes at the Voronoi nuclei and the intermediate points of particle boundaries, as shown in **Fig. 6**. Then, a simplified one-dimensional diffusion equation using truss elements is employed to carry out mass transfer. A mass transfer analysis based on RBSN and the truss networks model, in which truss elements are generated between the Voronoi nuclei, was proposed by Bolander (Bolander *et al.* 2003). This is one of the differences with the proposed model. A feature of this study is that it assumes the position of the node of truss elements on intermediate points of the particle boundaries, as mentioned in section 3.5.

3.2. Basic concept of diffusion equation

In the truss networks model, nonstationary potential flow problems are governed by Equation (4) below, a one-dimensional diffusion equation.

$$\frac{\partial \phi}{\partial t} = \frac{\partial}{\partial x}\left(D \frac{\partial \phi}{\partial x} \right) \tag{4}$$

where ϕ = some potential quantity such as the relative humidity and D = diffusivity.

D is variously referred to in the case of Fourier's, Fick's and Darcy's law, depending on the types of diffusivity. This can be expressed as a matrix,

$$\frac{AD}{L}\begin{bmatrix} 1 & -1 \\ -1 & 1 \end{bmatrix}\begin{Bmatrix} \phi_1 \\ \phi_2 \end{Bmatrix} + \frac{1}{\omega}\frac{AL}{6}\begin{bmatrix} 2 & 1 \\ 1 & 2 \end{bmatrix}\begin{Bmatrix} \partial\phi_1/\partial t \\ \partial\phi_2/\partial t \end{Bmatrix} + A\begin{Bmatrix} \phi_1 - \overline{\phi_1} \\ \phi_2 - \overline{\phi_2} \end{Bmatrix} = \begin{Bmatrix} 0 \\ 0 \end{Bmatrix} \tag{5}$$

where ϕ_1, ϕ_2 = potential quantity at each node, A = area of each truss element which is equal to the area of the corresponding Voronoi facet, and L = length of each truss element. The parameter ω in the second term is added to convert the volume of Voronoi to the volume of truss elements due to the overlap volume of adjacent truss elements, as shown in **Fig. 7** and Equation (6). This parameter is set as 2.0 for two-dimensional arrangement.

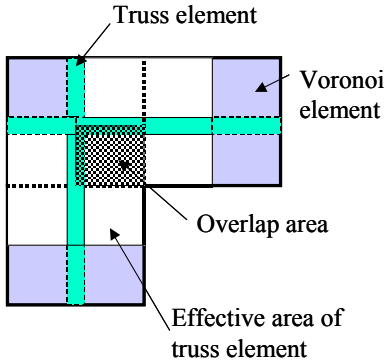

Fig. 7 Definition of overlap area and parameter omega (ω).

$$\omega = \frac{\sum_{i=1}^{n} A_i \cdot L_i}{V_{real}} \tag{6}$$

where n = total number of elements, A_i = cross-sectional area of each truss element, L_i = length of each truss element, i = element number and V_{real} = volume of the structure.

When several mass transfers are considered, they have relations to each other. Thus, the truss networks for each mass transfer are superposed and the various properties relate to each other. For example, the effective diffusion coefficient of chloride ions in the truss networks is assumed to depend on the relative humidity obtained from the truss networks of moisture transfer.

3.3. Moisture transfer

External drying shrinkage generally occurs in concrete members as soon as the formwork is removed. The difference between water loss by external drying and chemical hydration is, therefore, extreme when water diffusion of early age concrete is the highest. Since the area where the moisture content decreases shrinks, internal stress is induced, which in turn causes tensile stress at the surface of the specimen depending on the internal and external restraints. A diffusion equation using Darcy's law can describe the moisture transfer as follows.

$$\frac{\partial R}{\partial t} = \frac{\partial}{\partial x}\left(D_w \frac{\partial R}{\partial x} \right) \tag{7}$$

where R = relative humidity, t = time and D_w = moisture conductivity. The equation is solved by the initial condition and the following boundary condition.

$$\frac{\partial R}{\partial n} + \alpha_m \left(H_s + H_0 \right) = 0 \tag{8}$$

where n = normal vector of drying surface, α_m = moisture transmission coefficient, and H_S, H_0 = relative humidity of the drying surface and atmosphere, respectively. In this study, D_w is assumed as a constant value for simplicity.

3.4. Chloride ions penetration

Chloride ion penetration is one of the major problems that affect the durability of reinforced concrete structures. Although chloride ions in concrete do not directly cause severe damage to the concrete, they contribute to the corrosion of embedded rebars in the structure. The general diffusion equation can be written from Equation (4) using Fick's law, as shown in Equation (9). Thus, it is assumed that the diffusion coefficient changes according to the relative humidity (Saeki *et al.* 1996).

$$\frac{\partial C}{\partial t} = \frac{\partial}{\partial x}\left(D_{cl}^{'} \frac{\partial C}{\partial x} \right) \tag{9}$$

$$\frac{D_{cl}^{'}}{D_{cl0}} = 0.0032 \times 10^{0.025R} \tag{10}$$

where C = concentration of chloride ions, t = time, D'_{cl} = effective chloride ion diffusion coefficient, D_{cl0} = diffusion coefficient in water logged condition, and R = relative humidity.

3.5. Mass transfer through crack

The truss networks connected between the Voronoi nuclei and the intermediate points of the particle boundaries are expressed for the mass transfer within bulk concrete. Steel corrosion due to mass transfer through cracks, especially chloride ion diffusion, is, however, more important for structural performance. When surface cracks occur in reinforced concrete structures due to drying shrinkage or load application, chloride ions penetrate into the structure through these cracks. As described in the previous section, cracks will occur and propagate along the particle boundaries. To consider mass transfer through cracks in addition to through the bulk concrete, the truss networks are generated on particle boundaries in which a diffusion coefficient from that of the concrete material is assumed and the cross sectional area is varied by the crack width, as shown in **Fig. 8**. The diffusion coefficient of mass transfer through cracks may be quite large compared with that of bulk concrete.

Before cracking, the cross sectional area of truss elements on the particle boundaries is 0 and no mass transfer occurs in these truss elements. After cracking, the crack width can be calculated directly from the relative displacement between rigid particles. Therefore, the cross sectional area of the truss elements on the particle boundaries can be evaluated by multiplying the relative displacement with the thickness of the Voronoi element and mass can transfer along these truss elements in the concrete.

3.6. Checking efficiency of truss networks model

This section describes the application of the JCMAX thermal stress analysis program developed by the JCI Committee on Computer Code Development for Crack Control in Massive Concrete Using Finite Element Method (JCI committee, 2005) to analyze heat transfer in concrete specimens. The results of temperature distribution obtained from JCMAX were compared with the results of the truss networks model. The thermal diffusion can be described from Equation (11) using Fourier's law as follows:

$$\frac{\partial T}{\partial t} = \frac{\partial}{\partial x}\left(K \frac{\partial T}{\partial x} \right) \tag{11}$$

where T = temperature, t = time, and K = temperature diffusion coefficient.

Figure 9 displays the geometry of a specimen with 1500 Voronoi elements for the truss networks model and 100 rectangular elements for FEM analysis. **Table 1** lists the thermal properties of the concrete (thermal conductivity, heat transfer coefficient, specific heat and mass density). The initial and surrounding temperatures were set to 20°C and 0°C, respectively. For the boundary condition of heat transfer, higher temperatures inside the specimen can be transferred to the outside only via the heat transfer boundary using the truss networks gener-

Table 1 Thermal properties of concrete.

Thermal conductivity (W/m·K)	2.7
Heat transfer coefficient ($W/m^2 K$)	14
Specific heat (KJ/kg·K)	1.1
Mass density (kg/m^3)	2650

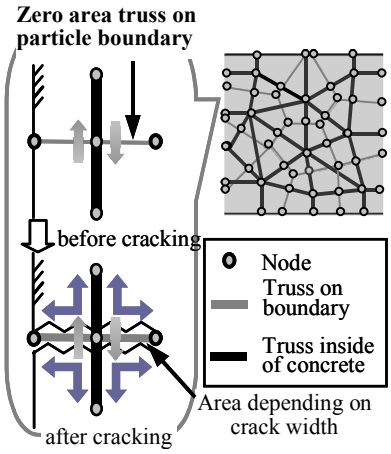

Fig. 8 Truss networks at crack.

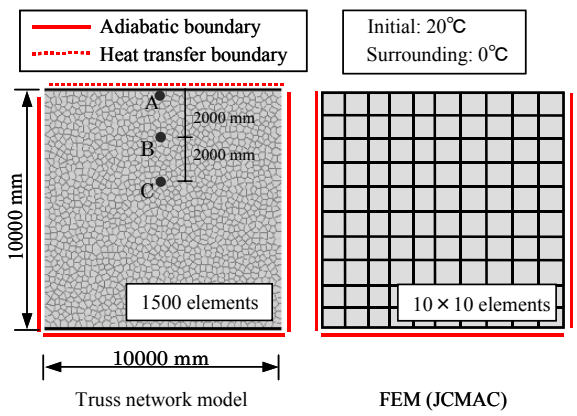

Fig. 9 Analytical model.

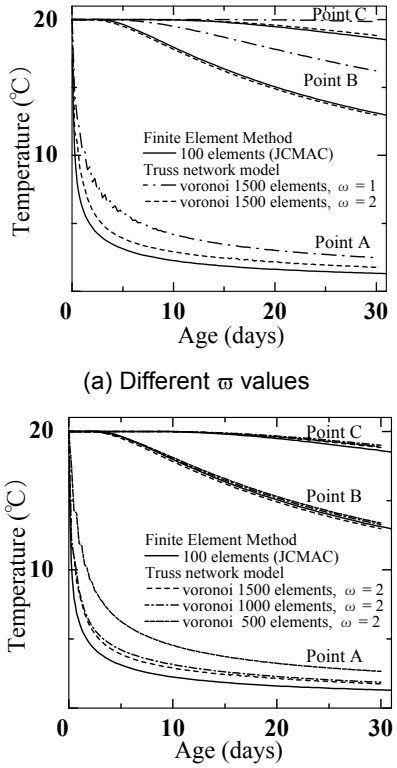

(a) Different ϖ values

(b) Different element numbers

Fig. 10 Comparison results.

ated between the Voronoi nuclei.

Figure 10 (a) compares the temperature distribution obtained from JCMAX and the truss networks model of points A, B and C. Two values of the conversion coefficient, ω (ω = 1 and 2), were used for analysis and comparison with the JCMAX program. The temperature distributions in which ω is set to 2.0 obtained from the truss networks model were found to closely agree with the results from the JCMAX program. Therefore, the truss networks model with Voronoi random mesh can be applied to analyze mass transfer for which ω is set to 2.0 for two-dimensional arrangements.

To investigate the effect of the number of elements, specimens divided into 500, 1000 and 1500 Voronoi elements were analyzed by using the truss networks model and setting ω to 2.0. **Figure 10 (b)** shows the comparison results between 500, 1000 and 1500 Voronoi elements for the truss networks model and 100 rectangular elements for the JCMAC program. Based on the results, a small mesh for calculating mass transfer by using the truss networks model is necessary to obtain the same results with FEM due to the difference in shape function.

4. Unification with structural analysis and mass transfer analysis

4.1. Internal stress due to drying shrinkage

Internal strain occurs in concrete due to the distribution

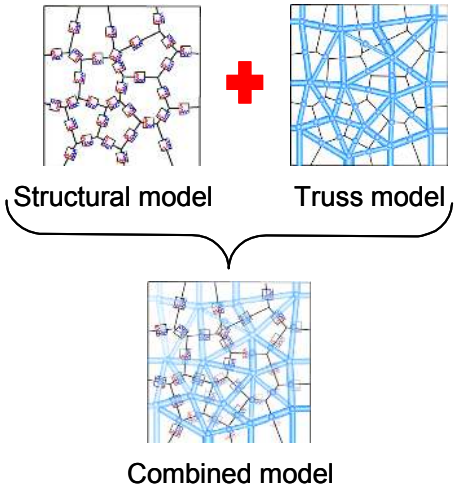

Fig. 11 Concept of unified model.

of the mass as a result of mass transfer. In the case of drying shrinkage, a linear relationship between the change in relative humidity, ΔR, and the corresponding change in shrinkage strain, $\Delta\varepsilon_n$, is assumed:

$$\Delta\varepsilon_n = \alpha_{sh}\Delta R \tag{12}$$

where α_{sh} = shrinkage coefficient.

Internal stress also occurs due to internal restraint from the internal strain distribution and external restraint from the boundary condition. The internal strain of each truss element obtained from mass transfer analysis is introduced to the corresponding normal springs of RBSN as structural analysis. **Figure 11** shows the unified model of the structural analysis and the mass transfer analysis used in the analysis. The matrix form of structural analysis is as follows. It solves the initial stress program taking into consideration time-dependent strain.

$$\iiint [B]^T [D^{ep}][B]\{d\}dV =$$

$$\iint [N]^T \{f\}dS + \iiint [B]^T [D^{ep}]\{\varepsilon^t\}dV \tag{13}$$

where $[D^{ep}]$ = elastic-plastic constitutive matrix and ε^t = time-dependent strain obtained from the mass transfer analysis.

4.2. Internal stress due to corrosion expansion of rebar

Cracks due to corrosion expansion of rebars are one of the major causes of deterioration. It is usually assumed that corrosion starts when the concentration of chloride ions at the surface of rebars exceeds a threshold value. In this study, the threshold value is set to 1.2×10^{-6} g/mm^3 (JSCE 2002) by unit volume of concrete and the corrosion velocity is set to 3.0×10^{-8} g/mm^2 day for simplicity.

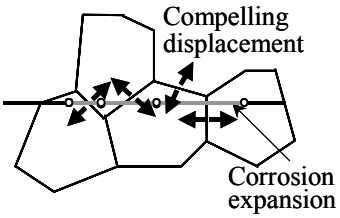

Fig. 12 Corrosion expansion.

Then, the compelling displacement induced by corrosion expansion is calculated by the following equation (Matsuo *et al.* 1997),

$$U = \frac{W_r (dV - 1)}{\rho_s} \tag{14}$$

where U = compelling displacement, W_r = corrosion volume of rebar, ρ_S = density of steel, and dV = volume expansion ratio of rust, set to 2.5.

The compelling displacement is translated to the displacement in the direction of normal springs at adjacent points, as shown in **Fig. 12**, and the internal strain is introduced in the springs which are calculated by dividing the displacement depending on the corrosion expansion by the normal spring length.

5. Crack propagation analysis due to drying shrinkage

5.1. Analysis outline

Drying shrinkage analysis is performed by considering the moisture transfer. **Figure 13** displays dog bone shape specimens (160 × 100 × 1000 mm) for free drying shrinkage analysis (free analysis) and 1-axial restrained analysis (restrained analysis) to investigate the effect of internal and external restraint, respectively. In the analysis, both specimens were divided by 1000 Voronoi elements.

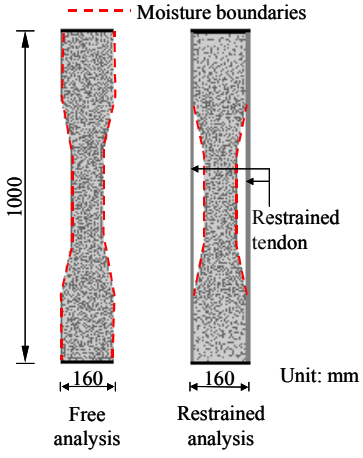

Fig.13 Analysis model.

Table 2 Concrete properties.

	A1	A2
Tensile strength, f_t (MPa)	3.0	
Young modulus, E (MPa)	2.00×10^4	
Moisture diffusivity within bulk concrete, D_w (mm^2/day)	10	30
Water transfer coefficient, α_m (mm/day)	30.0	
Shrinkage coefficient, α_{sh}	0.001	
Moisture diffusivity between cracks, D_{cr} (mm^2/day)	1.0×10^5	1.0×10^5
	0	

The analysis conditions are as follows. For boundary condition of free analysis and restrained analysis, vertical displacement at the bottom of the specimen was fixed. Humidity conditions of the atmosphere as boundary conditions for mass transfer analysis were set uniformly along both sides for free analysis and only along the bottleneck area for restrained analysis. The relative humidity of specimens was 100% at the initial stage. The relative humidity of the atmosphere was constant at 80% until 80 days and gradually decreased to 40% in the final stage (total testing period of 200 days). **Table 2** lists the material properties of A1 and A2. In the free analysis model, A1 and A2 were used to investigate the effect of internal restraint by setting different values of moisture conductivity, namely 10 and 30 mm^2/day, respectively. For the restrained analysis, the condition of A1 was applied and the restraint of the steel tendon was set to 100% and 200% by the rigidity ratio shown in the following equation. It should be noted that the moisture conductivity through cracks was assumed as the high value.

$$rigidity\ ratio = \frac{E_S A_S}{E_C A_C} \tag{15}$$

where E_s and A_s = Young's modulus and cross-sectional area of steel, respectively, E_c and A_c = Young's modulus and cross-sectional area of concrete at the middle section of the specimen, respectively.

5.2. Free drying shrinkage analysis (free analysis)

Figure 14 shows the change in free drying shrinkage strain for specimens A1 and A2 used for the free analysis. The average strains rapidly occurred at the beginning due to the different relative humidity values inside and outside the specimens. The rate of average strain then gradually decreased over time until 80 days. To accelerate the drying shrinkage strain, the relative humidity of the atmosphere was set to decline after 80 days. There-

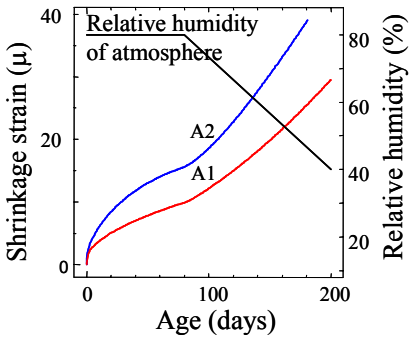

Fig. 14 Free drying shrinkage strain.

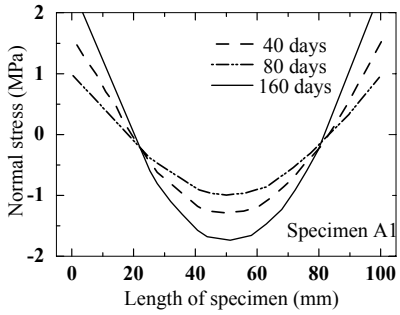

a) Specimen A1

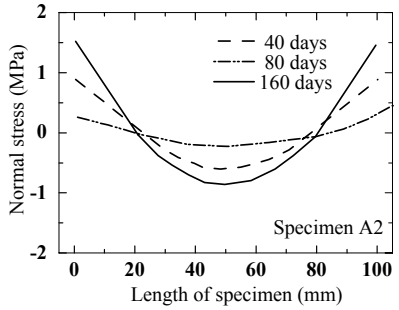

b) Specimen A2

Fig. 16 Profile of normal stress.

fore, normal shrinkage strains still occurred continuously. Specimen A2, which had a higher moisture conductivity value within bulk concrete obtained a higher average strain than specimen A1.

The relative humidity and normal stress distributions that occurred inside the specimens are indicated in **Fig. 15**. Note that due to the difference in relative humidity inside the specimens, tensile stresses occurred on the surface and many micro cracks occurred at 160 days due to the effect of internal restraint. For the normal stress profile of both specimens at 40, 80, and 160 days, as shown in **Fig. 16**, normal stress of specimen A1 was higher than that of A2 because specimen A1 has smaller moisture conductivity and shows a larger gradient of relative humidity content. Therefore, low moisture conductivity generates higher internal restraint.

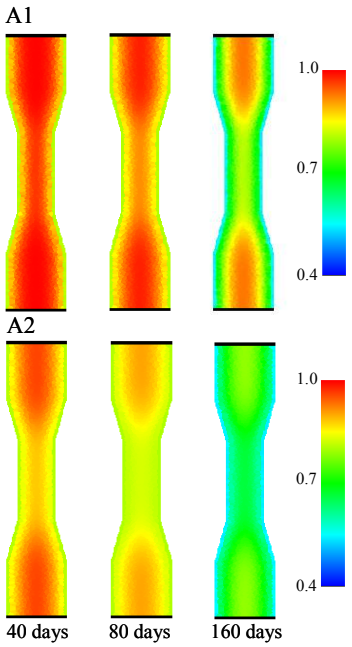

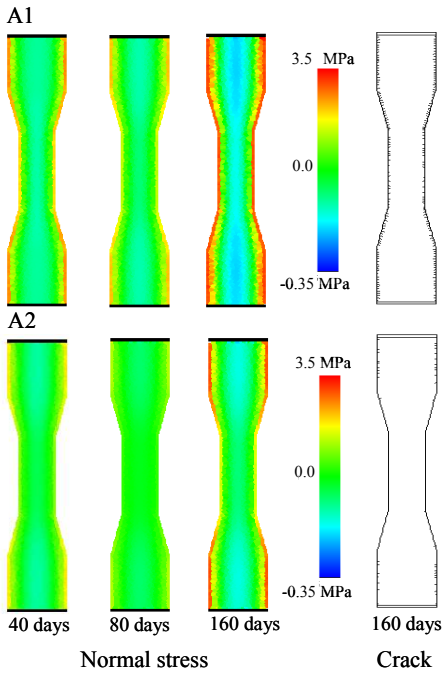

Fig. 15 Conditions inside specimens.

5.3. Uniaxial restrained analysis (restrained analysis)

The averaged strain that occurred in restrained tendons is shown in **Fig. 17**. In case of the high-restrained rate of 200%, through crack occurred at earlier age and the averaged strain has a small value. When the through crack occurs, the strain of the tendon becomes almost zero due to the release of restrained stress. **Figure 18** shows the relative humidity distributions and crack pat-

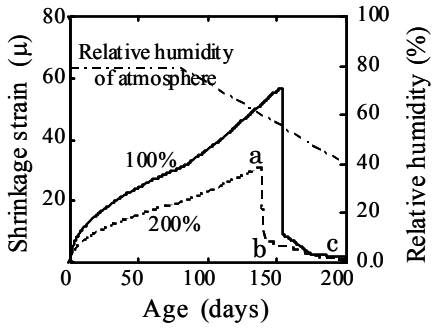

Fig.17 Average strain.

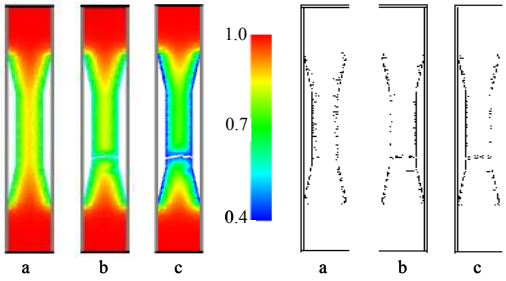

Fig.18 Relative humidity and crack pattern.

terns before and after through crack occurrence for the 200% restrained specimen, with a, b, c corresponding to marks a, b and c in **Fig. 17**.

Many cracks occurred on the surface, then cracks propagated into the specimen and the crack widths gradually increased. The specimen dehydrated according to the distance between both sides and the crack plane. Further, irregular relative humidity distribution on the surface occurred due to the occurrence of many surface cracks through which moisture was transferred.

6. Crack propagation Analysis due to drying shrinkage and corrosion

6.1. Analysis outline

Reinforced concrete bars as shown in **Fig. 19** were simulated by time-dependent structural analysis considering moisture transfer and chloride ion penetration with corrosion expansion of rebars. The specimen size is 200 × 200 × 1000 mm. A single rebar was placed at the center, with a reinforcement ratio of 1.0% for specimen A1, and two rebars were placed near the specimen surfaces with a reinforcement ratio of 2.0% for specimen A2. Specimen A1 and A2 were analyzed in two-dimensions with 1000 and 1500 Voronoi elements, respectively. The material properties are listed in **Table 3**.

For steel corrosion analysis (corrosion analysis) in which only chloride ion penetration is assumed, specimen A1 was analyzed. For moisture transfer and chloride ion penetration (coupled analysis), specimens A1 and A2

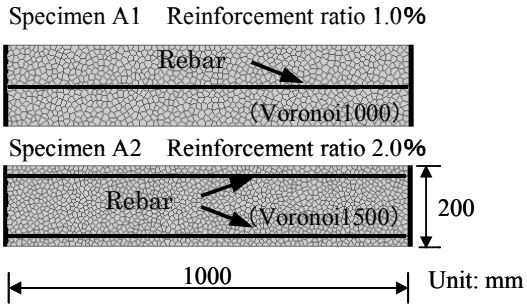

Fig. 19 Analytical model.

Table 3 Material properties.

Concrete (MPa)	Tensile strength, f_t	2.0
	Compressive strength, f_c	30.0
Rebar (MPa)	Yield strength, f_y	300.0
	Young's modulus, E_s	2.0×10^5
Moisture transfer (mm^2/day)	Moisture diffusivity within bulk concrete, D_w	10.0
	Moisture diffusivity between cracks, D_{crw}	1.0×10^5
Chloride ion penetration (mm^2/day)	Diffusion coefficient at water logged condition, D_{cl0}	8.00
	Diffusion coefficient between cracks, D_{crc}	8.0×10^5

were analyzed. The threshold value was set to 1.2×10^{-6} g/mm^3 at the initial corrosion. The diffusion coefficients of chloride ions and moisture conductivity through cracks were assumed to be high values. The diffusion coefficient of chloride ions within bulk concrete was set to 10 times the typical value in order to accelerate corrosion. For the boundary condition of structural analysis, the displacement in the horizontal direction for one end was fixed. On the other hand, only displacement in the vertical direction along specimen sides was assumed as the boundary condition for mass transfer analysis. Relative humidity and chloride ion concentration of specimens at the initial stage were 1.0 and 0.0 g/mm^3, respectively. The relative humidity of the atmosphere was set to 0.8 during the period of 0 to 200 days and 0.6 afterward until 600 days. The chloride ion concentration at the surface was set to 2.5×10^{-6} g/mm^3 for all periods.

6.2. Steel corrosion analysis (corrosion analysis)

In this case, only chloride ion penetration was considered. The distribution of stress in the lateral direction and crack patterns of specimen A1 are shown in **Fig. 20**. Cracks occurred along the rebar on both sides of the rebar because chloride ions transfer into the specimen uniformly due to the absence of surface cracks. Tensile stress and micro-cracks occurred around the steel bar at 360 days and major cracks occurred at 400 days.

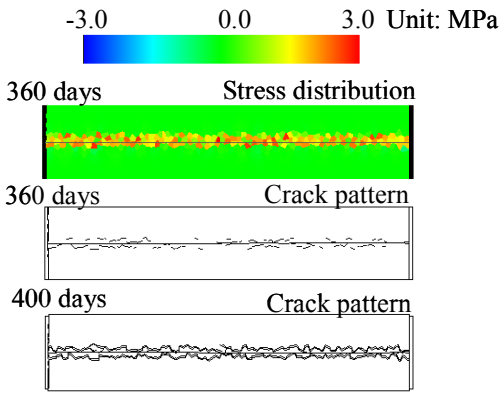

Fig. 20 Steel corrosion analysis.

6.3. Humidity and steel corrosion analysis (coupled analysis)

Specimen A1: **Figure 21** shows cracking behaviors, the distributions of relative humidity and the concentration of chloride ions at 50, 250 and 600 days obtained from the developed analysis method. At 50 days, many micro-cracks occurred at the specimen surface due to the effect of drying shrinkage. The soluble chloride ions gradually penetrated into the specimen via the boundary surface and the surface cracks. At 250 days, more shrinkage cracks occurred and major cracks reached the rebar, which led to diffusion of moisture and chloride ions through the cracks, causing corrosion of the rebar. At 600 days, mass transfer through cracks accelerated because of the increase in crack widths.

Moreover the cracks propagated along the rebar, since the specific concentration of chloride ions at the surface of rebar exceeded the threshold value. The analysis simulated well structural damages due to mass transfer. The crack patterns were different from the corrosion analysis due to the effect of drying shrinkage, because drying shrinkage can induce cracks on the surface and soluble chloride ions can penetrate through existing cracks. Thus, corrosion started locally near the cracks.

Specimen A2: In this case, proper covering and the effect of chloride ions on the concrete covering were considered, as shown in **Fig. 22**. Cracks occurred not only at the specimen surface due to drying shrinkage but also along the rebar due to the corrosion expansion of the rebar. When the concentration of chloride ions along both surfaces became higher than the threshold value, spalling of the concrete covering occurred. As shown in **Fig. 22**, spalling of concrete occurred at 262, 323 and 374 days for 2, 2.5 and 3 cm covering, respectively. Therefore, the thicker the covering, the longer the required slip off period and the longer the length.

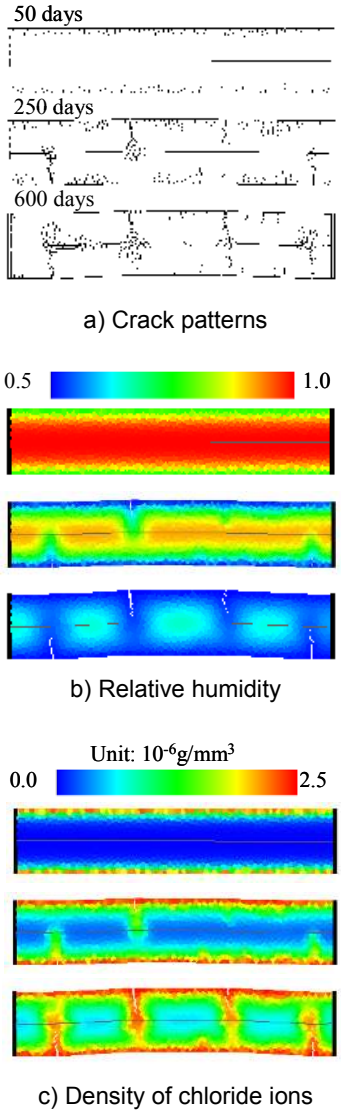

Fig. 21 Combined analysis of drying shrinkage and corrosion.

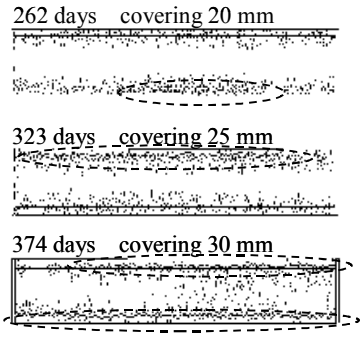

Fig. 22 Crack patterns of Specimen A2.

7. Load application analysis

7.1 Analysis outline

The geometry of the beam specimen, which was modeled with 1500 Voronoi elements, is shown in **Fig. 23**. The corrosion rate was set to the constant of 3.0×10^{-8} g/mm^2/day for all elements.

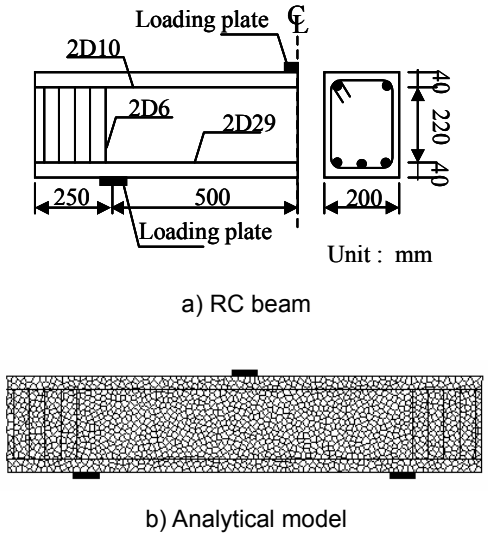

Fig. 23 Geometry and dimensions of RC beam.

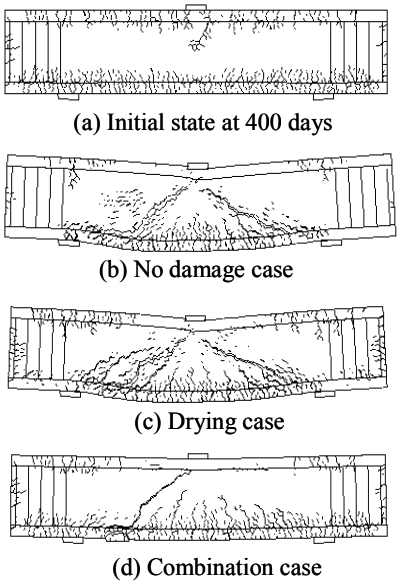

Fig. 25 Crack patterns and deformations.

Beam specimens were analyzed considering the combined effect of shrinkage and steel corrosion before load application (coupled-load analysis). The whole surface of the specimen except the surface of the loading plate was assumed as the boundary condition of mass transfer analysis. The relative humidity of the atmosphere was set to 0.4 during the period of 0 to 200 days and 0.6 afterward until 400 days. The other conditions were the same as described in section 6.1. It should be noted that the deterioration of material properties was not considered even in the damaged specimens. The load application analysis was performed for three cases: 1) Load application at 0 days for undamaged beam (undamaged), 2) Load application at 400 days for damaged beams, with only moisture transfer (drying) taken into consideration, and 3) Consideration of both moisture transfer and chloride ion penetration (combination).

7.2 Coupled-load analysis

Figure 24 shows the load displacement relation for three cases and **Fig. 25** shows deformations and crack patterns at the maximum load and at the initial state before loading at 400 days. For damaged beams, the load gradually decreased during mass transfer, since the displacement of the loading plate was numerically fixed by the displacement control. Different behaviors can be observed in each of the three cases. The initial slope of the load displacement relationship for the damaged beam becomes smaller than that of the undamaged beam. This is the effect of the initial cracks due to the mass transfer. **Figure 25 (a)** shows the initial state at 400 days for the combination case. Many cracks occurred on the surface of the specimen due to drying shrinkage and corrosion expansion of the rebar. For the drying case, the maximum load shows a larger value than that of the undamaged case. This is the reason why the initial cracks obstructed the propagation of diagonal cracks. This situation is often observed in the test in which initial damage is introduced. For the combination case, the load dropped suddenly when the diagonal crack propagated. And, spalling of the cover concrete occurred at the same time. The deterioration of structural performance was simulated in the developed method.

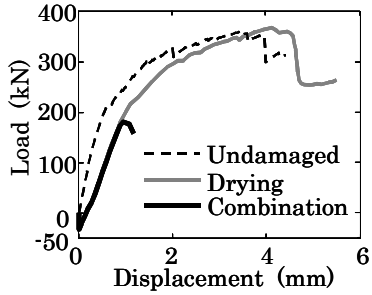

Fig.24 Load-displacement relationship.

8. Conclusions

This paper reports the development of a newly developed unified analytical method with load application analysis for short-term behavior and mass transfer analysis for long-term behavior. The Rigid-Body-Spring Networks model was used for structural analysis and the truss networks model was utilized for mass transfer analysis. As the mass transfer through bulk concrete and cracks, moisture transfer and soluble chloride ion penetration were adopted. Then, deterioration processes such as the cracking behavior under multi actions in consideration of drying shrinkage and rebar corrosion expansion were

simulated, taking into consideration the effect of mass transfer through cracks. The analysis was found to simulate well structural damages as well as deterioration process due to mass transfer. Moreover, a damaged structure due to mass transfer was analyzed under external load, and the deterioration of structural performance was simulated with the developed method.

As the proposed model is under the first stage of development, the prime objectives of this paper are to propose and to verify the possibility of the new numerical model. Realizing the importance of creep and autogenous shrinkage as time-dependent behavior and degradation of material properties such as bond strength, the authors will conduct further studies to consider these issues in greater detail.

References

Bolander, J. E. and Berton, S. (2003). "Simulation of shrinkage induced cracking in cement composite overlays." *Cement and Concrete Composites*, 26 (7), 861-871.

Bolander, J. E. and Saito, S. (1998). "Fracture analysis using spring networks with random geometry." *Engineering Fracture Mechanic*, 61. 569-591.

Comite Euro-International du Beton, CEB-FIP Model Code 1990.

JCI. (2005). "Japan Concrete Institute Computer Program of Thermal Stress Analysis for Massive Concrete Structure (JCMAC)." Tokyo: Japan Concrete Institute.

JSCE. (2002). "Standard specifications for concrete structure-Structural Performance Verification." Tokyo: Japan Society of Civil Engineers.

Kawai, T. (1978). "New discrete models and their application to seismic response analysis of structures." *Nuclear Engineering and Design*, 48. 207-229.

Kitoku, T., Higai, T and Saito, S. (2005). "The effect of cover concrete and bar diameter on the bond stress-slip relation of deformed bars." *Proceedings of the Japan Concrete Institute*, 27 (2). 757-762. (in Japanese)

Matsuo, T. *et al*. (1997). "Crack propagation analysis of concrete dependent on expansion of reinforcement." *Proceedings of the Japan Concrete Institute*, 19 (2). 99-104. (in Japanese)

Nakamura, H. and Higai, T. (2001). "Compressive fracture energy and fracture zone length of concrete." In: *Modeling of inelastic behavior of RC structures under seismic loads*. ASCE: 471-487.

Saeki, T. and Niki, H. (1996). "Migration of chloride ions in non-saturated mortar." *Proceedings of the Japan Concrete Institute*, 18 (1). 969-974. (in Japanese)

Saito, S. and Bolander, J. E. (1997). "Numerical analysis of shrinkage cracking controlled by carbon fiber nets." *Proceedings of 3rd International Symposium on Non-Metallic (FRP) Reinforcement for Concrete Structures*, Sapporo, Japan, 2. 275-282.

Saito, S. and Hikosaka, H. (1999). "Numerical analyses of reinforced concrete structures using spring networks models." *Journal of Materials, Concrete Structures and Pavements*, JSCE, 672 (44). 289-303.

Shima, H. and Okamura, H. (1987). "Bond-slip-strain relationship of deformed bars embedded in massive concrete." *Journal of Materials, Concrete Structures and Pavements*, JSCE, 378 (6). 165-174. (in Japanese)

Ueda, M., Takeuchi, H., Higuchi, H. and Kawai, T. (1984). "A discrete limit analysis of reinforced concrete structures." *In Computer-Aided Analysis and Design of Concrete Structure*, eds. Damjanic, F., Hinton, E., Owen, D. R. J., Bicanic, N. and Simovic, V., Pineridge Press, Swansea, UK, 1369-1384.